Articles

Kinetic Modeling and Determination of Reaction Constants of Alzheimer's β-Amyloid Fibril Extension and Dissociation Using Surface Plasmon Resonance†

Kazuhiro Hasegawa,*,‡ Kenjiro Ono,§ Masahito Yamada,§ and Hironobu Naiki‡

Department of Pathology, Fukui Medical University, Fukui 910-1193, Japan, and Department of Neurology and Neurobiology of Aging, Kanazawa University Graduate School of Medical Science, Kanazawa 920-8640, Japan

Received May 17, 2002

ABSTRACT: To establish the kinetic model of the extension and dissociation of β-amyloid fibrils (fAβ) in vitro, we analyzed these reactions using a surface plasmon resonance (SPR) biosensor. Sonicated fAβ were immobilized on the surface of the SPR sensor chip as seeds. The SPR signal increased linearly as a function of time after amyloid β-peptides (Aβ) were injected into the fAβ-immobilized chips. The extension of fAβ was confirmed by atomic force microscopy. When flow cells were washed with running buffer, the SPR signal decreased with time after the extension reaction. The curve fitting resolved the dissociation reaction into the fast exponential and slow linear decay phases. Kinetic analysis of the effect of Aβ/fAβ concentrations on the reaction rate indicated that both the extension reaction and the slow linear phase of the dissociation were consistent with a first-order kinetic model; i.e., the extension/dissociation reactions proceed via consecutive association/dissociation of Aβ onto/from the end of existing fibrils. On the basis of this model, the critical monomer concentration ($[M]_e$) and the equilibrium association constant (K) were calculated, for the first time, to be 20 nM and 5×10^7 M^{-1}, respectively. Alternatively, $[M]_e$ was directly measured as 200 nM, which may represent the equilibrium between the extension reaction and the fast phase of the dissociation. The SPR biosensor is a useful quantitative tool for the kinetic and thermodynamic study of the molecular mechanisms of fAβ formation in vitro.

The deposition of Alzheimer's β-amyloid fibrils (fAβ)[1] in the brain has been suggested to play a central role in the pathogenesis of Alzheimer's disease (AD), probably as an early event in the amyloid cascade (*1*−*3*). Attempts to reduce the fAβ deposited in the brain using peptide vaccine or low molecular weight compounds, in addition to the prevention of fAβ deposition, are under extensive investigation (*4*−*8*). Amyloid fibril formation is considered as a protein misfolding and aggregation event, in which the non-native conformer of the precursor protein is thermodynamically stabilized by template-dependent accumulation (*9*). Therefore, biophysical investigations, especially from the standpoint of the protein structure and thermodynamics, are essential to elucidate the mechanism of amyloid fibril formation.

Several groups have proposed a nucleation-dependent polymerization model to explain the mechanisms of fAβ formation in vitro (*7*, *10*−*16*). This model consists of two phases, i.e., nucleation and extension phases. Nucleus formation requires a series of association steps of amyloid β-peptides (Aβ), which are thermodynamically unfavorable, representing a rate-limiting step in amyloid fibril formation. Once the nucleus (*n*-mer) has been formed, further addition of Aβ becomes thermodynamically favorable, resulting in a rapid extension of amyloid fibrils. We and other groups have independently developed a first-order kinetic model of fAβ extension in vitro and confirmed that the extension of fAβ proceeds via the consecutive association of Aβ onto the ends of existing fibrils (*13*−*16*). This model indicates that the net rate of fAβ extension is the sum of the rates of polymerization and depolymerization. At the critical monomer concentration (equilibrium monomer concentration, $[M]_e$), the rates of polymerization (extension) and depolymerization (dissociation) are balanced, and fibrils do not extend or depolymerize. On the basis of this model, the inverse of $[M]_e$ corresponds to the equilibrium association constant (K), i.e., the ratio of dissociation and association rate constants.

Unlike other protein interactions, amyloid fibril formation is an infinite reaction concerning the reaction site, which is continuously created by the association of precursor proteins. Therefore, determination of $[M]_e$ is the only way to calculate

† This research was supported in part by Grant-in-Aid for Scientific Research on Priority Areas (C), Advanced Brain Science Project, from the Ministry of Education, Culture, Sports, Science, and Technology of Japan.

* Corresponding author. Tel: 081-776-61-8321. Fax: 081-776-61-8123. E-mail: khase@fmsrsa.fukui-med.ac.jp.

‡ Department of Pathology, Fukui Medical University.

§ Department of Neurology and Neurobiology of Aging, Kanazawa University Graduate School of Medical Science.

[1] Abbreviations: Aβ, amyloid β-peptides; AD, Alzheimer's disease; AFM, atomic force microscopy; fAβ, β-amyloid fibrils; fAβ(1−40), fAβ formed from Aβ(1−40); $[M]_e$, critical monomer concentration; RU, response unit; SPR, surface plasmon resonance; ThT, thioflavin T.

10.1021/bi020369w CCC: $22.00 © 2002 American Chemical Society
Published on Web 10/26/2002

K. Utilizing a closed system with thioflavin T (ThT) fluorometric assay, we previously estimated $[M]_e$ and *K* of fAβ extension at pH 7.5 in the presence of 1 M urea to be 10 μM and 10^5 M^{-1}, respectively (*13*). To elucidate the detailed mechanisms of amyloid fibril formation in vitro, we need to observe directly the depolymerization reaction and determine the kinetic and thermodynamic constants. However, the dissociation reaction of fAβ is not usually observed in a closed system in a physiological buffer condition using the ThT assay, possibly because of the low $[M]_e$ of the extension reaction (less than the order of micromolar) (*4*). Therefore, the flow cell system to wash out the released monomer from the reaction site is required for detecting precisely the dissociation of fAβ in the physiological buffer solution.

Myzka et al. (*18*) demonstrated that the surface plasmon resonance (SPR) biosensor is useful for the analysis of the extension and dissociation reaction of fAβ at an Aβ concentration less than 10 μM. The experimental system using an SPR biosensor has several advantages for monitoring the kinetics of fAβ extension and dissociation in vitro: (1) no modification or labeling is required for the detection of Aβ, (2) a continuous flow cell system keeps the Aβ concentration constant during the extension reaction and keeps the Aβ concentration below $[M]_e$ during the dissociation reaction by washing out the released Aβ, (3) the reaction can be monitored in real time with a time resolution of 0.1−1 s intervals. With this paradigm, they observed the fast and slow phases of the dissociation reaction and suggested that fAβ extension can be explained by a "dock-lock" mechanism consisting of the reversible and irreversible association steps of Aβ onto the ends of fAβ (*17*). However, they did not characterize the detailed kinetic aspects of the reaction, including the effect of Aβ/fAβ concentrations on the extension/dissociation rates. These studies may be essential to obtain several kinetic and thermodynamic constants, thus to establish kinetic and thermodynamic models of fAβ extension/dissociation in vitro.

In this study, we confirmed that the increase in SPR signals corresponds to the extension of fAβ by observing the surface of the sensor chip by atomic force microscopy (AFM). We also analyzed the extension/dissociation kinetics of fAβ to obtain several kinetic and thermodynamic constants. We propose that the extension/dissociation reaction of fAβ in this SPR system can be explained by a first-order kinetic model, as well as by a dock-lock model.

EXPERIMENTAL PROCEDURES

Preparation of Aβ and fAβ Solutions. Aβ(1−40) (trifluoroacetate form, code 4307-v, lot no. 501001; Peptide Institute, Inc., Osaka, Japan) were dissolved by brief vortexing in 0.02% ammonia solution at a concentration of about 500 μM (2.2 mg/mL) in a 4 °C room and stored at −80 °C before assaying (fresh Aβ solution). The solution was clear, and no fibrillar components were observed by electron microscopy (data not shown). No significant ThT fluorescence was detected by fluorescence spectroscopy. Additionally, 50 μM Aβ was incubated in 50 mM phosphate buffer, pH 7.5, and 100 mM NaCl at 37 °C; spontaneous fAβ formation was not observed at least for 10 days.

fAβ(1−40) were formed from freshly dissolved Aβ(1−40) (HCl form, code 4379-v, lot no. 501005; Peptide Institute, Inc., Osaka, Japan) solution as described above. The reaction mixture (1000 μL) containing 50 μM Aβ(1−40), 50 mM phosphate buffer, pH 7.5, and 100 mM NaCl was incubated for 8 h at 37 °C without agitation. After incubation, 5% NaN_3 was added to yield 0.05% and stored at 4 °C without sonication. After the centrifugation of the stock solution at 4 °C for 2 h at $(1.6 \times 10^4)g$, the supernatant contained no Aβ, confirming that the extension reaction was completed with no Aβ remaining in the solution.

Immobilization of fAβ on the Sensor Chip of the BIAcore Biosensor. Freshly extended fAβ were prepared just before immobilization. Stored fAβ were diluted with 7 volumes of water and sonicated on ice with 20 intermittent pulses (pulse, 0.6 s; interval, 0.4 s; output level, 2) using an ultrasonic disruptor (UD-201; Tomy, Tokyo, Japan) equipped with a microtip (TP-030; Tomy, Tokyo, Japan). The reaction mixture in an Eppendorf tube was 950 μL and contained 50 μM Aβ (trifluoroacetate form), 5 μg/mL (equivalent to 1.2 μM Aβ) sonicated fAβ, 50 mM phosphate buffer, pH 7.5, and 100 mM NaCl. After incubation at 37 °C for 24 h, the mixture was centrifuged at 4 °C for 2 h at $(1.6 \times 10^4)g$. fAβ had precipitated completely as measured by the fluorescence of ThT. The pellet was resuspended in water, sonicated as described above, and then immobilized immediately on the pioneer sensor chip F1 (BIAcore AB, Uppsala, Sweden) by amine coupling. The F1 chip has a shorter (carboxymethyl)dextran chain (approximately 30 nm) on the surface than the CM5 chip (approximately 100 nm). The (carboxymethyl)dextran surface was activated with a 70 μL injection of a mixture of *N*-ethyl-*N*′-(3-dimethylaminopropyl)carbodiimide hydrochloride and *N*-hydroxysuccinimide at a flow rate of 5 μL/min. The sonicated fAβ(1−40) was diluted with 10 mM sodium acetate (pH 4.0) at concentrations between 9 and 18 μg/mL and then injected until the desired immobilization level was achieved. The remaining activated groups were blocked with a 70 μL injection of 1 M ethanolamine (pH 9.0). BIAcore 1000 and 3000 are equipped with four flow cells in one sensor chip. Various densities of fAβ were immobilized on flow cells 2, 3, and 4. The reference cell (flow cell 1) was prepared by the above-described amine coupling without addition of fAβ.

SPR Analysis of fAβ Extension and Dissociation. The SPR experiments were performed with BIAcore 1000 and 3000 (BIAcore AB). BIAcore 3000 was used to monitor both the extension and dissociation reactions, while BIAcore 1000 was used to monitor the extension reaction only. The reaction was performed at 37 °C, unless otherwise noted, using the PBS running buffer (50 mM phosphate, pH 7.5, 100 mM NaCl, 3 mM EDTA, 0.005% Tween 20). The running buffer was continuously degassed with an online degasser (model SD8023; Tosoh Corp., Tokyo, Japan) throughout analysis. Aβ was diluted to 0.1−30 μM with the running buffer. For the extension reaction, 10−250 μL of Aβ(1−40) solutions was injected into flow cells using a KINJECT mode at a flow rate of 30 μL/min. In BIAcore 3000, the same Aβ solution flows through all four flow cells on the sensor chip. For the dissociation reaction, the sensor chip was washed with running buffer for 60 or 120 min after the end of injection.

Calculation of the Extension and Dissociation Kinetics. The data were processed using BIAevaluation 3.1. To correct the instrumental noise and bulk reflective change, each of the sensorgrams of flow cells 2−4 was subtracted by the sensorgram of a blank cell (flow cell 1) obtained by the simultaneous measurement. When the samples of low concentrations were analyzed in the extension reaction, the sensorgrams were compensated using the "double referencing" (*19*), since the fluctuation during injection was significant and dependent on the amount of immobilized fibrils. The sensorgram obtained at the load of the sample solution was first referenced by the sensorgram of a blank cell. This sensorgram was further subtracted by the sensorgram of the identical cell obtained at the load of the running buffer, which was also referenced by the sensorgram of a blank cell. The extension rate was calculated as the slope of the linear curve fitting to the extension phase. For the dissociation phase, the sensorgram was subtracted only by the sensorgram of the blank cell (flow cell 1), since the subtraction by the sensorgram of the running buffer will cancel the intrinsic dissociation itself. The response signal of the initial period of dissociation (0−100 s after the end of injection) was discarded because of the fluctuation. Noises derived from the flow fill of the syringe pump were also removed. The kinetic parameters of the dissociation phase were calculated by the curve fitting of the compensated sensorgram using Igor Pro version 4 (WaveMetrics, Inc., Lake Oswego, OR).

Direct Measurement of [M]$_e$. For the extension reaction, 30 μL of 1 or 3 μM Aβ solution was first injected, followed immediately by the injection of 240 μL of 0−1 μM Aβ solution using COIJNECT mode. To cancel the intrinsic fluctuation caused by the injection, the sensorgrams were processed by the double referencing as described above. As a result of double referencing, the sensorgrams indicated only the fast exponential phase of the dissociation reaction vide infra.

First-Order Kinetic Model of fAβ Extension and Dissociation. As reported previously, the kinetic properties of amyloid fibril extension can be described as

$$[\mathrm{P}] + [\mathrm{M}] \underset{k_{\mathrm{off}}}{\overset{k_{\mathrm{on}}}{\rightleftharpoons}} [\mathrm{P}] \quad (1)$$

where [P] is the number concentration of seed fibrils, [M] is the concentration of monomeric or dimeric Aβ, and k_{on} and k_{off} are the apparent rate constants for polymerization (extension) and depolymerization (dissociation), respectively (*13*). If t is the reaction time and $f(t)$ is the concentration of Aβ which has newly polymerized into fAβ during the reaction, then eq 1 can be written as

$$f'(t) = k_{\mathrm{on}}[\mathrm{P}][\mathrm{M}] - k_{\mathrm{off}}[\mathrm{P}] = (k_{\mathrm{on}}[\mathrm{M}] - k_{\mathrm{off}})[\mathrm{P}] \quad (2)$$

where $f'(t)$ represents the rate of fAβ extension at a given time and k_{on}[P][M] and $-k_{off}$[P] denote the rate of polymerization and depolymerization, respectively. $[\mathrm{M}]_e$ can be obtained by setting $f'(t)$ in eq 2 equal to zero to obtain

$$[\mathrm{M}]_{\mathrm{e}} = k_{\mathrm{off}}/k_{\mathrm{on}} = 1/K \quad (3)$$

where K is the equilibrium association constant.

ThT Fluorescence Spectroscopy. All studies were performed essentially as described elsewhere (*13*) on a Hitachi F-4500 fluorescence spectrophotometer. Optimum fluorescence measurements of fAβ were obtained at the excitation and emission wavelengths of 445 and 490 nm, respectively, with the reaction mixture containing 5 μM ThT (Wako Pure Chemical Industries, Ltd., Osaka, Japan) and 50 mM glycine−NaOH buffer, pH 8.5. Fluorescence was measured immediately after making the mixture and was averaged for the initial 5 s.

AFM. fAβ was immobilized on a C1 sensor chip (BIAcore) in which the carboxymethyl residue was directly coupled to the gold thin layer with no dextran chain. Sonicated fAβ were first immobilized onto the surface of flow cells 2 and 3 with a density of 900 response units (RU). A 5 μM Aβ solution was injected into flow cell 3 until the response increased by 900 RU to 1800 RU. The glass support of the sensor chip was then removed from the plastic support by dissolving the adhesives with ice-cold acetone. The AFM images of the sensor chip surface were obtained with a dynamic force microscope (SPI-3800N-SPA400; Seiko Instruments) equipped with a scanning microcantilever (SI-DF20; Seiko Instruments) at a scan rate of 0.5 Hz. The length of fibrils was measured manually on the printouts. Student's t-test was used for statistical analysis.

Other Analytical Procedures. Protein concentrations of Aβ and fAβ solutions were determined by the method of Bradford (*20*) using a protein assay kit (500-0001; Bio-Rad Laboratories, Inc., Hercules, CA). Throughout this study, the Aβ solution quantified by amino acid analysis was used as the standard. For the statistical evaluation of linearity, linear regression and correlation coefficients were calculated using Microsoft Excel version 98.

RESULTS

AFM Imaging of the Fibrils on the Sensor Chip. The extension of immobilized fAβ was directly observed by AFM (Figure 1). Sensor chip C1 was used for imaging to avoid the roughness of the dextran-coated surface on sensor chip F1. The average length of the fibrils in an area of 4 × 4 μm^2 was 152 ± 74 nm (n = 241) and 265 ± 142 nm (n = 226) for seed fibrils (flow cell 2) and extended fibrils (flow cell 3), respectively. The average length of fAβ on flow cell 3 was doubled ($p < 0.001$) by the extension reaction, well explaining the increase of SPR response (900 RU to 1800 RU). Moreover, the number of the fibrils in a 4 × 4 μm^2 area remained roughly unchanged (n = 241 vs 226).

Reproducibility of the Extension Reaction. The reproducibility of the extension reaction was examined by two different protocols. In protocol 1 (A), fAβ were extended by the 50 μL injection of a 10 μM Aβ solution, followed by the dissociation reaction with the running buffer for 60 min. As shown in Figure 2A, when Aβ was injected onto immobilized fAβ, the SPR response increased linearly without a lag phase. At the dissociation phase, the SPR response decreased continuously even at the end of the dissociation reaction (60 min). As shown in Figure 5, the curve fitting analysis resolved the dissociation phase into the fast exponential and slow linear phases. While the fast exponential phase ended within 30 min, the slow linear phase continued at the end of the dissociation reaction (60 min). Thus, the next cycle was started after 60 min of the dissociation and repeated 10 times. As shown in Figure 3A,B,

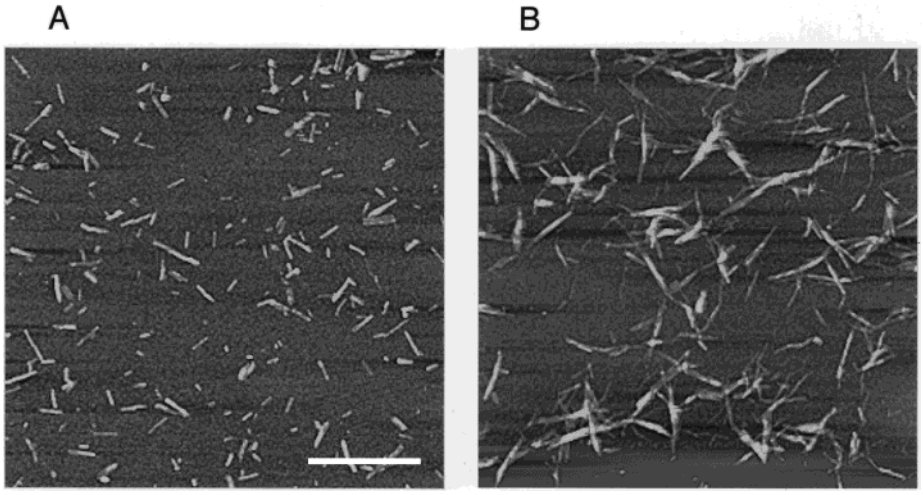

FIGURE 1: AFM image of fAβ on the sensor chip. Sonicated fAβ were immobilized on the surface of flow cells 2 (A) and 3 of the sensor chip C1 with a density of 900 RU. A 5 μM Aβ solution was injected into flow cell 3 until the response increased by 900 RU to 1800 RU (B). Then the surface of flow cells 2 and 3 was scanned using AFM as described in Experimental Procedures. The bar indicates a length of 1 μm.

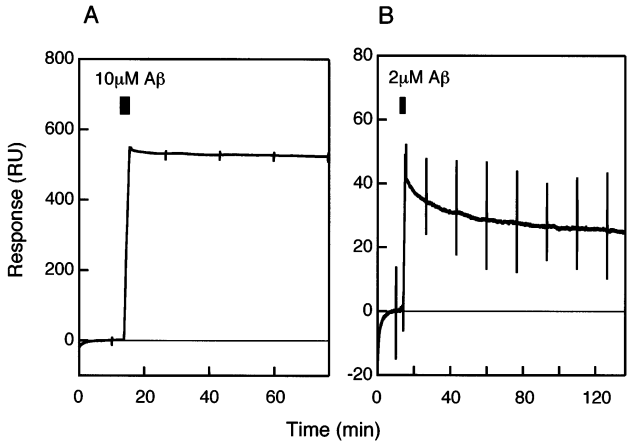

FIGURE 2: Time course of the extension and dissociation of fAβ. Sonicated fAβ were immobilized on the flow cells at a density of 2000 RU. In protocol 1 (A), fAβ were extended by a 50 μL injection of a 10 μM Aβ solution, followed by the dissociation reaction with the running buffer for 60 min. In protocol 2 (B), fAβ were extended by a 30 μL injection of a 2 μM Aβ solution, followed by the dissociation reaction with the running buffer for 120 min. The plot was created by adjusting the response (RU) at 100 s before the start of the injection to $y = 0$.

the rate of the extension reaction decreased during the early cycles but was relatively stabilized after several repetitions.

We performed the following studies to search for the reason the extension rate decreased cycle dependently, as well as to confirm that we observe the same phenomenon at every cycle.

First, the effect of the density of immobilized fAβ, i.e., the number concentration of the fibril [P] in every cycle, was examined by replotting the data in Figure 3B. As shown in Figure 3C, a linear correlation of the reaction rate with [P] was maintained throughout the cycles. This may indicate that the reduction of the response in every cycle is similar among three flow cells, irrespective of the immobilized fAβ density.

Second, the detachment of fAβ from the surface of flow cells was examined. When all flow cells were extensively washed at a high flow rate ("unclogging" command), the decrease in SPR response (RU) was 0.087 $\pm$ 0.019% of the immobilized fAβ (RU) for all flow cells. Since this change is similar to the decrease observed without unclogging (0.12 $\pm$ 0.046%), detachment of covalently bound fAβ may be negligible.

Finally, to keep the fibril length as constant as possible, fibrils were extended by a short length and then extensively dissociated with protocol 2. In this protocol (Figure 2B), fAβ were extended by a 30 μL injection of 2 μM Aβ, followed by the dissociation reaction with the running buffer for 120 min. As shown in Figure 2B, the increase in response by the extension reaction was decreased to half by the dissociation reaction. Since 2000 RU of fAβ was immobilized on the chip, the increase in the 40 RU response corresponds to a 2% increase in the average length of fAβ. As shown in Figure 3D, the reduction rate of the response in every cycle is much smaller than that in protocol 1.

All of these results may indicate that the reduction of the response in every cycle may be caused by the cumulative extension of the fibrils cycle by cycle. This mechanism will be discussed later. To minimize the effect of repetition, we performed all kinetic analyses after the stabilization by five to ten repetitions. To monitor the reduction of response signals, we injected the same Aβ solution at the beginning and the end of each session. If the reduction was evident, the response signal was compensated by assuming the linear reduction cycle by cycle. Moreover, as Figure 3C indicates, a direct comparison of the response among three flow cells may be reasonable if all flow cells are used simultaneously by the same protocol after several repetitions.

Effect of Aβ and fAβ Concentration on the Extension Rate. When various concentrations of Aβ were injected sequentially into the flow cells, a good linearity was observed between the Aβ concentration and the extension rate in each flow cell (Figure 4A,B). Similarly, when the Aβ concentration was constant, the extension rate was linear in relation to the density of immobilized fAβ (Figure 4C). The apparent extension rate constant k_{on} was calculated using eq 2. Since [P] is constant and $k_{on}[M] \gg k_{off}$ during the extension reaction, $k_{on}[P]$ (RU s^{-1} M^{-1}) can be approximated by the extension rate/[M]. [P] is unable to be determined as an absolute unit. However, when the same fAβ were im-

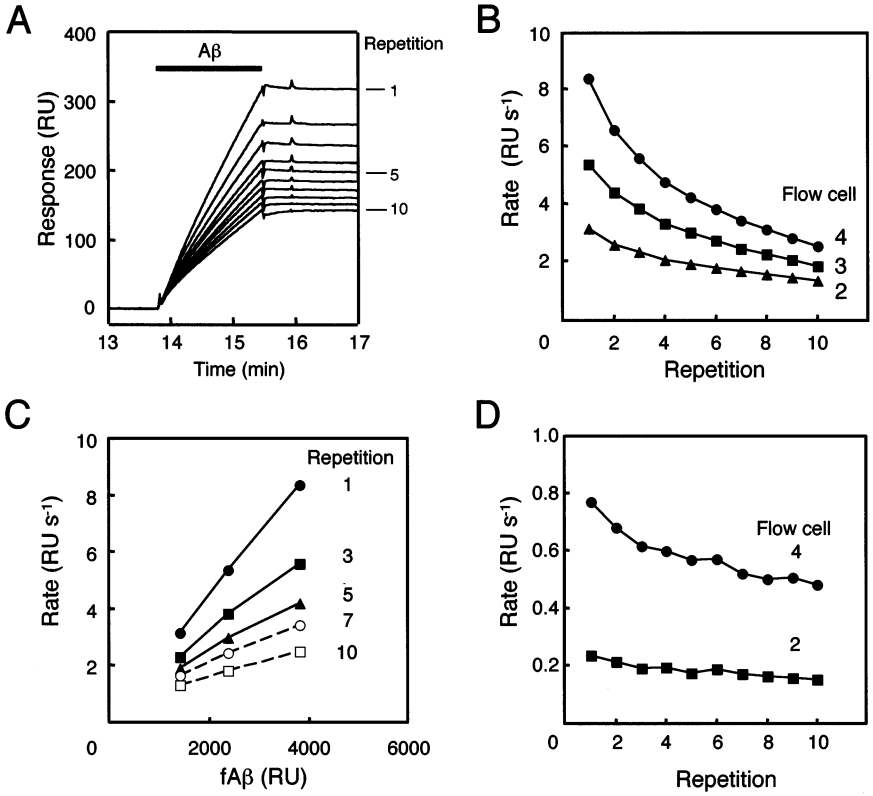

FIGURE 3: Reproducibility of the extension reaction. (A) Time course of the extension reaction during the repetition with protocol 1. A 10 μM Aβ solution (50 μL) was injected into a flow cell on which 1000 RU of fAβ was immobilized. The overlay plot was created by adjusting the response (RU) at 100 s before the start of the injection to $y = 0$. (B) Effect of the repetition (protocol 1) on the extension rate. Extension rates were calculated as described in Experimental Procedures and then plotted against the number of repetitions. fAβ were immobilized on flow cells 2 (▲), 3 (■), and 4 (●) at a density of 1400, 2370, and 3810 RU, respectively. All flow cells were analyzed simultaneously. (C) Effect of the repetition (protocol 1) on the correlation between the extension rate and immobilized fAβ density. The extension rates in (B) were replotted against the fAβ density on each flow cell. Extension rates of the repetition cycle 1 (●), 3 (■), 5 (▲), 7 (○), and 10 (□) were displayed. (D) Effect of the repetition (protocol 2) on the extension rate. Extension rates were plotted as in (B). fAβ were immobilized on flow cells 2 (■) and 4 (●) at a density of 615 and 2020 RU, respectively. These flow cells were analyzed simultaneously.

mobilized on all flow cells, [P] should be proportional to the density (RU) of immobilized fAβ. When k_{on}[P] obtained from the data between 3 and 20 μM Aβ in Figure 4B was divided by the density (RU) of immobilized fAβ, the averaged values were 107.5 ± 5.2, 117.0 ± 11.7, and 122.9 ± 2.58 s^{-1} M^{-1} for flow cells 2, 3, and 4, respectively. Thus, it may be reasonable to consider the calculated apparent k_{on} as a constant.

Dissociation Kinetics. The dissociation kinetics was examined in the same experiment of the extension reaction with protocol 1. At the first three times of a series of reactions, the running buffer was injected into all flow cells. As shown in Figure 5A, the sensorgrams obtained by the repeated injection of the running buffer completely overlapped with each other. These sensorgrams fitted well with a linear decay model, and the slopes of the linear fit were proportional to the density of immobilized fAβ [$(-1.96 \pm 0.19) \times 10^{-3}$, $(-3.90 \pm 0.24) \times 10^{-3}$, and $(-5.98 \pm 0.18) \times 10^{-3}$ RU s^{-1} for flow cells 2, 3, and 4, respectively; slope (RU s^{-1}) = (-1.57×10^{-6})fAβ, $r = 0.995$].

When 1−30 μM Aβ were injected into flow cells sequentially, the decrease in the response was dependent on both the Aβ concentration and the density of immobilized fAβ (Figure 5). Curve fitting analyses using the single exponential or linear decay model did not fit well these dissociation sensorgrams (data not shown). Thus, these sensorgrams were fitted with two different biphasic models. The first model is described by a rate equation $R_{L+E}(t)$ composed of exponential and linear decay components as a function of time (t):

$$R_{L+E}(t) = N_0 - k_{d1}(t - t_0) + N_{fast}e^{-k_{d2}(t-t_0)} \qquad (4)$$

where k_{d1} and k_{d2} denote the apparent dissociation constants of linear decay and exponential decay, respectively, N_{fast} denotes the coefficient of exponential decay, N_0 denotes a signal offset, and t_0 denotes the start point of dissociation.

A series of dissociation sensorgrams of 1−30 μM Aβ for each flow cell were analyzed simultaneously using global curve fitting with common constants. The apparent rate constants and coefficients calculated from this analysis are summarized in Table 1 and Figure 6A, respectively. Similar results were obtained by the local curve fitting with separate constants (data not shown). As shown in Table 1, the constants of linear decay (k_{d1}) for each flow cell were proportional to the density of fAβ [k_{d1} (RU s^{-1}) = (1.65×10^{-6})fAβ, $r = 0.977$]. Interestingly, k_{d1} for each cell was similar to the decay rate observed by the injection of the running buffer, indicating that k_{d1} is the intrinsic rate constant depending only on the density of immobilized fAβ. On the other hand, the constants of exponential decay (k_{d2}) were relatively invariant among flow cells [half-life $t_{1/2}$ (ln 2/k_d) was 5.18, 6.88, and 8.43 min for flow cells 2, 3, and 4, respectively]. The coefficients for exponential decay (N_{fast})

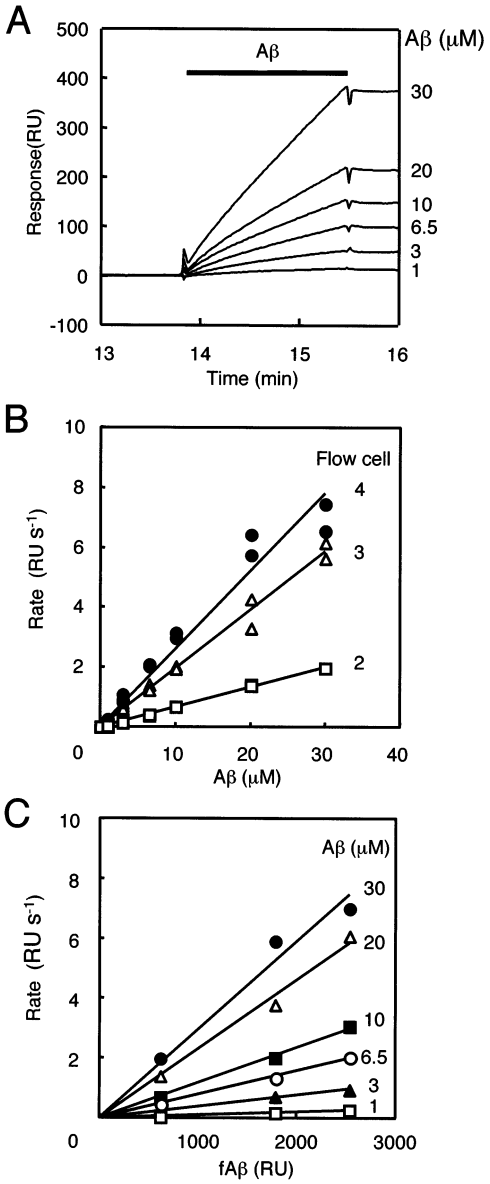

FIGURE 4: Effect of Aβ concentration and immobilized fAβ density on the extension rate. (A) Effect of the Aβ concentration on the time course of the extension reaction (protocol 1). Aβ at a concentration of 1−30 μM (50 μL) was injected into the flow cell on which 1000 RU of fAβ was immobilized. The overlay plot was created by adjusting the response (RU) at 100 s before the start of the injection to $y = 0$. (B) Effect of Aβ concentration on the extension rate. Extension rates were calculated and plotted against the Aβ concentration as described in Experimental Procedures. fAβ were immobilized on flow cells 2 (□), 3 (△), and 4 (●) at a density of 620, 1780, and 2530 RU, respectively. Correlation coefficients (r) of linear regression were 0.999, 0.995, and 0.983 for flow cells 2, 3, and 4, respectively. (C) Effect of immobilized fAβ density on the extension rate. The average of the extension rates in (B) was plotted against fAβ density. Correlation coefficients (r) of linear regression were 0.990, 0.995, 0.994, 0.996, 0.993, and 0.976 for 1 (□), 3 (▲), 6.5 (○), 10 (■), 20 (△), and 30 (●) μM Aβ, respectively.

were dependent on both the density of fAβ and the Aβ concentration (Figure 6A).

Other investigators used a double exponential model to analyze the dissociation reaction (*17*, *19*). For comparison, we also performed curve fitting using a rate equation $R_{DE}(t)$ as a function of time (t):

$$R_{DE}(t) = N_0 + A_1 e^{-\tau_1(t-t_0)} + A_2 e^{-\tau_2(t-t_0)} \qquad (5)$$

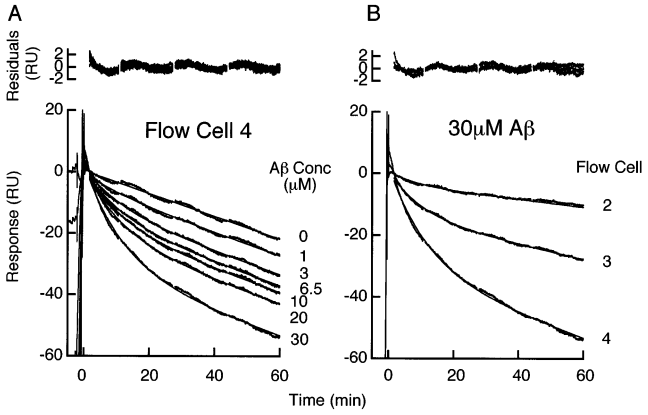

FIGURE 5: Time course of the dissociation reaction. (A) Aβ at a concentration of 0−30 μM (50 μL) was injected into flow cell 4 on which 3810 RU of fAβ was immobilized. The three sensorgrams obtained by the repeated injection of the running buffer completely overlapped with each other. (B) A 30 μM Aβ solution (50 μL) was injected into flow cells 2, 3, and 4 with the immobilized fAβ density of 1400, 2370, and 3810 RU, respectively. The sensorgrams were obtained and compensated as described in Experimental Procedures. The overlay plot was created by adjusting the end point of sample injection to $x = 0$ and then the response (RU) at 100 s after the end of the injection to $y = 0$. In both (A) and (B), the calculated curve using a rate equation $R_{L+E}(t)$ was overlayed on each sensorgram except for the three sensorgrams obtained by the injection of the running buffer, on which linear curve fitting was applied (A). Residuals of curve fitting, i.e., difference between calculated and observed values, for all cases were plotted on the upper panels of (A) and (B). The residuals were small throughout the dissociation, indicating that the curve fitting was appropriate. Each curve is a representative of duplicate or triplicate analysis for each concentration.

Table 1: Apparent Dissociation Kinetic Constants Calculated by Global Curve Fitting Using Rate Equations $R_{L+E}(t)$ and $R_{DE}(t)$

flow cell	$R_{L+E}(t)$		$R_{DE}(t)$	
	k_{d1} (RU s^{-1})	k_{d2} (s^{-1})	τ_1 (s^{-1})	τ_2 (s^{-1})
2	2.15×10^{-3}	2.23×10^{-3}	3.51×10^{-3}	1.83×10^{-4}
3	4.03×10^{-3}	1.68×10^{-3}	2.59×10^{-3}	1.10×10^{-4}
4	6.28×10^{-3}	1.37×10^{-3}	2.98×10^{-3}	1.77×10^{-4}

where τ_1 and τ_2 denote the apparent dissociation constants of the fast and slow exponential decay, respectively, and A_1 and A_2 denote the coefficients of the fast and slow exponential decay, respectively. As shown in Table 1, the apparent dissociation constants, τ_1 and τ_2, were relatively invariant among flow cells. While the coefficients for the fast exponential decay (A_1) were dependent on both the fAβ density and the Aβ concentration (Figure 6B), those for the slow decay (A_2) were dependent mostly on the fAβ density (Figure 6C). The apparent dissociation constant of the fast decay τ_1 ($t_{1/2} = 3.8$ min) is close to that of Myzka et al. (approximately 3 min) (*18*).

The coefficients N_{fast} and A_1 are similar (Figure 6A,B), and the apparent rate constants k_{d2} and τ_1 are also similar (Table 1) for each Aβ concentration and fAβ density. Therefore, the fast decay term of $R_{DE}(t)$ and the exponential decay term of $R_{L+E}(t)$ were comparable in their contribution to the total dissociation. The slow decay term of $R_{DE}(t)$ was also comparable to the linear decay term of $R_{L+E}(t)$. Indeed, k_{d1}/([P] in RU) and τ_2, both of which reflect the slow dissociation rate per fibril, are constant among flow cells 2−4 (Table 1). Thus, both biphasic decay models can well explain the observed dissociation curves. However, to

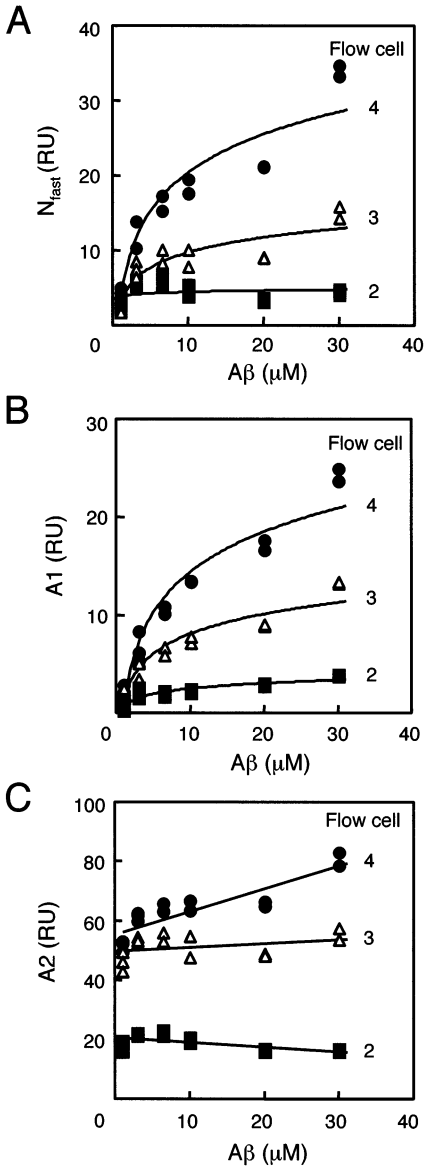

FIGURE 6: Calculated coefficients for each dissociation sensorgram obtained from the global curve fitting using rate equations $R_{L+E}(t)$ and $R_{DE}(t)$. Coefficients for flow cells 2 (■), 3 (△), and 4 (●) were plotted against Aβ concentration. N_{fast} (A) is a coefficient for the exponential decay phase of $R_{L+E}(t)$. A_1 (B) is a coefficient for the faster exponential decay phase of $R_{DE}(t)$. A_2 (C) is a coefficient for the slower exponential decay phase of $R_{DE}(t)$.

analyze the dissociation sensorgrams in the present study, we prefer to use the former model as described by eq 4, because the sensorgrams obtained by the injection of the running buffer fitted well with a linear decay model and the slopes of the linear fit were proportional to the density of immobilized fAβ.

To examine the effect of progressive stabilization of fAβ with time, the contact time was varied (20 s to 8.3 min) by the injection of 10−250 μL of 10 μM Aβ onto the immobilized fAβ (3100 RU) using protocol 1 at a constant flow rate of 30 μL/min. Similar to the effect of Aβ concentration as in Figure 5A, the decrease in the response was dependent on the contact time of the Aβ solution injected (Figure 7A). Global curve fitting analyses with common constants using a rate equation $R_{L+E}(t)$ fitted well with these dissociation sensorgrams ($k_{d1} = 2.38 \times 10^{-3}$ RU s^{-1} and $k_{d2} = 2.62 \times 10^{-3}$ s^{-1}), and the coefficient for the exponential

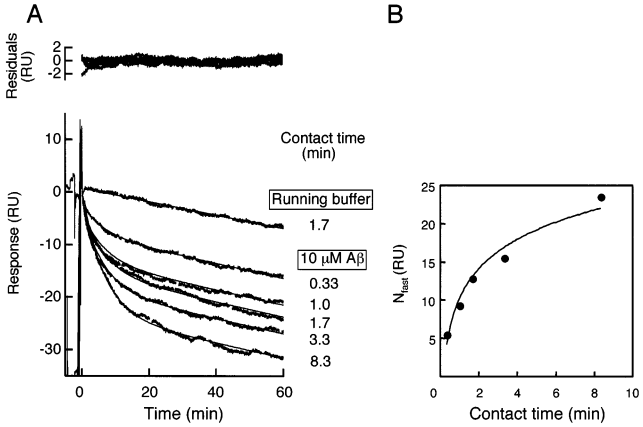

FIGURE 7: Effect of the contact time of Aβ onto the immobilized fAβ. (A) Time course of the dissociation reaction. The running buffer (50 μL) and 10−250 μL of 10 μM Aβ were injected into the flow cell on which 3100 RU of fAβ was immobilized. The sensorgrams were obtained and compensated as described in Experimental Procedures. The overlay plot of the dissociation reaction and residuals was created as described in Figure 5, except that the response (RU) at 50 s after the end of the injection was to $y = 0$. The calculated curve using a rate equation $R_{L+E}(t)$ was overlayed on each sensorgram except for the sensorgram obtained by the injection of the running buffer, on which linear curve fitting was applied. (B) Coefficients N_{fast} plotted against the contact time. The calculated k_{d1} and k_{d2} were 2.38×10^{-3} RU s^{-1} and 2.62×10^{-3} s^{-1}, respectively.

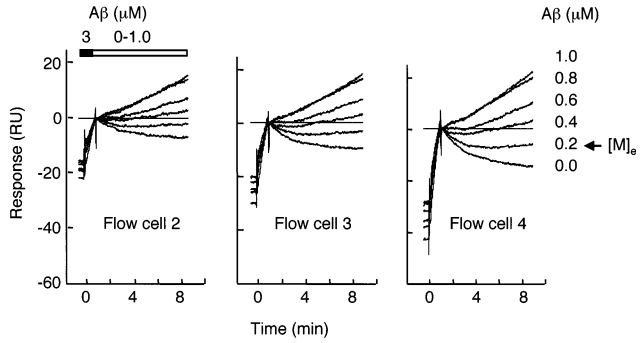

FIGURE 8: Direct measurement of $[M]_e$. A 3 μM Aβ solution (30 μL) was injected into flow cells, followed immediately by the injection of 240 μL of a 0−1 μM Aβ solution. fAβ were immobilized on flow cells 2, 3, and 4 at a density of 1400, 2370, and 3810 RU, respectively. The sensorgrams were obtained and compensated as described in Experimental Procedures. The overlay plot was created by adjusting the start point of the first injection to $x = 0$ and then the response (RU) at the start point of second injection to $y = 0$.

decay (N_{fast}) increased by the increase of the contact time (Figure 7B). Additionally, the calculated k_{d1} of each sensorgram was the same as the linear decay constant of the sensorgram obtained by the injection of the running buffer (1.98×10^{-3} RU s^{-1}).

Critical Monomer Concentration. $[M]_e$ was obtained by two different procedures. First, $[M]_e$ was directly measured as shown in Figure 8. When the running buffer was injected after injection of 3 μM Aβ, a decrease in the response was observed. When the Aβ concentration of the second injection was 0.4 μM or more, an increase of the response was observed. At about 0.2 μM Aβ, the change in the response was not evident in the flow cells, suggesting that the extension rate and the dissociation rate were balanced independent of the immobilized fAβ density. Therefore, we assume 0.2 μM as $[M]_e$.

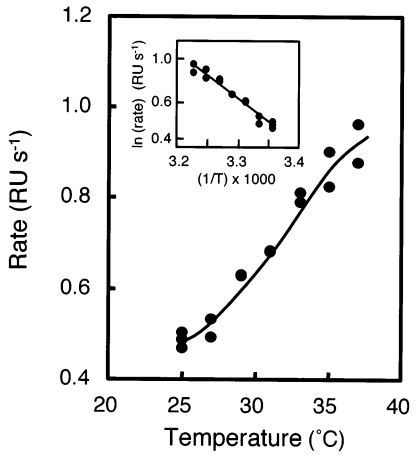

FIGURE 9: Effect of the incubation temperature on the rate of fAβ extension. For the extension reaction (protocol 2), 30 μL of a 3 μM Aβ solution was injected repeatedly to a flow cell (fAβ density: 2000 RU) by raising the temperature from 25 to 37 °C. This procedure was repeated twice, and the reduction of the extension rate by repetition was compensated by referring to the reduction of the response (RU) at 25 °C between two sessions. The inset shows the Arrehnius plot and T indicates the absolute temperature. Linear regression and correlation coefficients were calculated ($r = -0.982$).

Second, $[M]_e$ was calculated by the modified eq 3, i.e., $[M]_e = k_{off}[P]/k_{on}[P]$. When 50 μL of 3 μM Aβ solution was injected, the extension rates were 0.333, 0.473, and 0.701 RU s^{-1} for flow cells 2, 3, and 4, respectively. As described above, the apparent $k_{on}[P]$ can be approximated by the extension rate/[M] from eq 2. Therefore, the apparent $k_{on}[P]$ was calculated to be 1.11×10^5, 1.58×10^5, and 2.34×10^5 RU s^{-1} M^{-1} for flow cells 2, 3, and 4, respectively. If we presume the apparent dissociation rate constant $k_{off}[P]$ as the linear decay constant (k_{d1}) (RU s^{-1}) of $R_{L+E}(t)$ as described in Table 1, $[M]_e$ calculated from the modified eq 3 are 19.4 ± 1.3, 25.7 ± 2.0, and 27.0 ± 2.4 nM for flow cells 2, 3, and 4, respectively. The calculated $[M]_e$ is about $^1/_{10}$ of the directly measured $[M]_e$. The implications of these $[M]_e$ will be discussed later.

Effect of the Incubation Temperature on the Extension Rate. As shown in Figure 9, the extension rate was greatly dependent on the incubation temperature. The inset in Figure 9 shows an Arrhenius plot. This plot indicates that between 25 and 37 °C, a good linearity ($r = -0.983$) was observed between the natural logarithm of the extension rate and the reciprocal of the incubation temperature (represented by absolute temperature). Since the extension rate is approximated to $k_{on}[P][M]$, the natural logarithm of rate ln(rate) is expressed as

$$\ln(\text{rate}) = \ln k_{on} + \ln [P] + \ln [M] \qquad (6)$$

Then from the Arrhenius law, $\ln k_{on} = \ln A - E_a/RT$, eq 6 can be rewritten as

$$\ln(\text{rate}) = \ln [P] + \ln [M] + \ln A - E_a/RT \qquad (7)$$

where E_a is the activation energy, R is the gas constant, T is the absolute temperature, and A is the preexponential factor. From eq 7 and the slope of the Arrhenius plot, E_a is calculated as 42.9 kJ mol^{-1} (10.3 kcal mol^{-1}).

DISCUSSION

Stability of the Extension Reaction. The reduction of the response in every cycle may be caused by the cumulative extension of the fibrils cycle by cycle (Figure 3). As a characteristic of the SPR detection system, the evanescent wave penetrates the lower refractive index medium for out to about 300 nm, and the energy intensity decreases exponentially with the distance from the metal surface (*21*). In this experiment, freshly extended and sonicated fibrils were immobilized on the surface of the sensor chip. As shown in Figure 1A, the immobilized fibrils did not overlap with each other. Thus the fibril ends, where the extension and dissociation reaction could occur, may be close to the metal surface. According to the repetition of the reaction, entanglement of the fibrils as shown in Figure 1B would raise the fibril ends to the second or higher layers distant from the metal surface, thus making the sensitivity of the SPR signal lower in relation to the distance. This explanation is in good agreement with the above-described interpretation of Figure 3.

First-Order Kinetic Model of fAβ Extension. As shown in Figure 4A, the time course of the extension reaction was linear, and no other kinetic component was evident. Additionally, the rate of reaction was proportional to both the Aβ concentration ([M]) and the density of immobilized fAβ ([P]). These results are consistent with a first-order kinetic model of the extension reaction. This model was built on the assumption that [P] is constant; i.e., no seeds are generated during the reaction. When Aβ was injected into flow cell 1 on which no fAβ were immobilized, no increase in the response was observed. Moreover, the number of fibrils in a 4 × 4 μm^2 area remained roughly unchanged during the extension reaction (Figure 1). Therefore, we conclude that fAβ extended via the consecutive association of Aβ onto the ends of fAβ with no change in the number concentration of fAβ.

Dissociation Kinetics. By the curve fitting analysis, the dissociation reaction was divided into the fast and slow decay phases (see Figures 5 and 6 and Table 1). Other investigators also observed the fast and slow phases of the dissociation reaction (*17*, *18*). The half-life of the fast decay phase observed in this study (5.2−8.4 min) is similar to those obtained by other groups, 10.4 min (*17*) and 3 min (*18*). Therefore, our results may be explained by a dock-lock model, where the fast and slow decay phases may correspond to the "dock" and "lock" states, respectively (*17*, *18*). Esler et al. (*17*) investigated the association/dissociation of radioactive iodine-labeled Aβ to/from the synthetic fAβ immobilized on the bottom of the plate with a 100 pM order of Aβ. On the other hand, we and Myzka et al. (*18*) investigated the association/dissociation of Aβ to/from immobilized fAβ using a 10 μM order of Aβ, about 10^5 times higher concentration than that used by Esler et al. Thus, we cannot conclude that the data presented in this paper represent the same phenomena as observed by Esler et al. Further studies may be essential to elucidate the details of the transition state of Aβ during the template-dependent folding in the extension reaction.

As for the slow decay phase, other groups applied an exponential decay model to this phase, without establishing a definite kinetic model of the slow decay (*17*, *18*). We

applied a linear decay model represented by eq 4 to this phase and demonstrated that this phase ($-k_{d1}t$) can be explained by the dissociation term of a first-order kinetic model ($-k_{off}$[P]) in eq 2.

The possibility of progressive stabilization of fAβ with time was examined by varying the contact time (20 s to 8.3 min) of 10 μM Aβ onto the immobilized fAβ (Figure 7). Similar to the result of Myszka et al. (*18*), the increase of the contact time increased the dissociation rate (compare Figure 7 with Figure 5A in ref *18*). The result of curve fitting using a rate equation $R_{L+E}(t)$ indicated that the contact time-dependent increase of the dissociation rate was governed almost exclusively by the increase of the coefficient for the exponential decay (N_{fast}). On the other hand, the dissociation rate of the slow phase (k_{d1}) was constant at least for a few hours. Myszka et al. proposed the progressive stabilization of fAβ with time by normalizing the dissociation phase by setting the response at the start of the dissociation phase to 1 (see Figure 5B in ref *18*). If the slow dissociation rate were constant, this normalization would apparently reduce the dissociation rate. Thus, we currently conclude that the increase of the contact time may increase the amount of the fast phase of dissociation (the "dock state" component) but may not affect the slow phase of dissociation (the "lock state" component).

Equilibrium Constants and Energetics of the Reaction. As described above, the calculated $[M]_e$ was about $^1/_{10}$ of the directly measured $[M]_e$ (20 vs 200 nM). As a result of double referencing of the sensorgrams, the directly measured $[M]_e$ may probably represent the equilibrium between the extension reaction and the fast phase of dissociation (Figure 8).

By contrast, the calculated $[M]_e$ represents the equilibrium between the extension reaction and the slow phase of the dissociation; thus we can calculate K to be 5×10^7 M^{-1} with eq 3. The standard free energy change ($\Delta G°$) of the reaction can now be estimated using the equation:

$$\Delta G° = -RT \ln K \tag{8}$$

where R is the gas constant and T is the absolute temperature. $\Delta G°$ is calculated to be about 46 kJ mol^{-1} (11 kcal mol^{-1}) for calculated $[M]_e$. This $\Delta G°$ may correspond to the difference in the standard free energy between Aβ and fAβ. This $\Delta G°$ is close to the value estimated by Kusumoto et al. using the Arrehnius equation (about 7 kcal mol^{-1}) (*22*).

From the Arrehnius plot in Figure 9, the activation energy E_a was calculated to be 42.9 kJ mol^{-1} (10.3 kcal mol^{-1}), about half of the value calculated by Kusumoto et al. (23 kcal mol^{-1}) (*22*). Although we analyzed the extension reaction at pH 7.5, they analyzed in 0.1 M HCl (pH = 1). Therefore, this difference in the reaction condition may cause the difference in E_a.

Overall, the SPR biosensor system is a useful quantitative tool not only for the kinetic analysis but also for the thermodynamic analysis of the extension reaction. The van't Hoff analysis, measuring K by varying the reaction temperature, may reveal the enthalpy change ($\Delta H°_{vH}$). When we compare $\Delta H°_{vH}$ with the enthalpy change measured by calorimetry ($\Delta H°_{cal}$), the essential information on the conformational change during the extension will be obtained.

Biological Significance. Recently, some evidence has demonstrated that soluble oligomers of Aβ or protofibrils may be more toxic to neuronal cells than mature fAβ in the brains of AD patients as well as of AD animals (*23*). However, these findings may not rule out the role of mature fAβ on the development of AD. Additionally, even if mature fAβ represent the inactive reservoir of Aβ, rather than the prima donna of the toxic Aβ species, they may be important as a potential regulator of Aβ level in the brain.

Although the Aβ concentration in the cerebrospinal fluid was in the order of picomolar to nanomolar in AD and normal control groups (*24*), we and other groups used a micromolar order of Aβ in in vitro studies to study the mechanism of fAβ formation (*4*, *6*, *7*, *10*−*14*, *18*). Funato et al. (*25*) quantitated the concentration of insoluble Aβ(1−42) in many AD and control brains and found that significant amounts of insoluble Aβ(1−42) had already accumulated in the AD brains before the appearance of amyloid burden. The threshold concentration of insoluble Aβ(1−42) for amyloid burden was about 400 pmol/g (0.4 μM) in occipito-temporal cortex T4 and about 200 pmol/g (0.2 μM) in hippocampus CA1. These results suggest that Aβ peptides may be highly concentrated in the microenvironment before the start of fAβ deposition. Interestingly, these threshold values are close to $[M]_e$ obtained in the present study.

The Aβ level in the brain is regulated not only by the production of Aβ from β-amyloid precursor proteins but also by the proteolytic degradation of Aβ by neprilysin and other proteases (*26*). A first-order kinetic model suggests that fAβ formation in vivo would be regulated by the balance of the polymerization and depolymerization reactions. Therefore, reduction of the Aβ level in vivo by reducing the production or by increasing the degradation may prevent or retard fAβ deposition, not only by reducing the polymerization reaction but also by giving rise to the depolymerization reaction.

In conclusion, we demonstrated that both the extension reaction and the slow linear phase of the dissociation are consistent with a first-order kinetic model. On the basis of the model, we calculated the critical monomer concentration ($[M]_e$), the equilibrium association constant (K), and the standard free energy change ($\Delta G°$) for the first time. We believe that the experimental system described in this paper may prove useful to elucidate the detailed mechanism of fAβ formation in vitro. This system may also be potentially useful for the study of the effects of various biological substances and organic compounds on the extension and dissociation reactions of fAβ in vitro.

ACKNOWLEDGMENT

The authors gratefully acknowledge Drs. Kazuhiro Nagata, Nobuko Hosokawa, and Kazunori Hirayoshi, Institute for Frontier Medical Science, Kyoto University, for BIAcore instruments and discussion; Drs. Eiji Saji and Hiroyuki Magara, Industrial Technology Center of Fukui Prefecture, and Dr. Toshiya Nishimura, Seiko Instruments Inc., for AFM imaging; Dr. Issei Okazaki, Biacore K.K., for technical support and discussion; and Shinobu Tsutsumi, Hiromi Okada, Nobuo Takimoto, and Hitoshi Takagi for excellent technical assistance.

REFERENCES

1. Selkoe, D. J. (2001) *Physiol. Rev. 81*, 741−766.
2. Hardy, J. A., and Higgins, G. A. (1992) *Science 256*, 184−185.

3. Sommer, B. (2002) *Curr. Opin. Pharmacol. 2*, 87−92.
4. Ono, K., Hasegawa, K., Yoshiike, Y., Takashima, A., Yamada, M., and Naiki, H. (2002) *J. Neurochem. 81*, 434−440.
5. Findeis, M. A. (2000) *Biochim. Biophys. Acta 1502*, 76−84.
6. Naiki, H., Gejyo, F., and Nakakuki, K. (1997) *Biochemistry 36*, 6243−6250.
7. Naiki, H., Hasegawa, K., Yamaguchi, I., Nakamura, H., Gejyo, F., and Nakakuki, K. (1998) *Biochemistry 37*, 17882−17889.
8. Janus, C., Pearson, J., McLaurin, J., Mathews, P. M., Jiang, Y., Schmidt, S. D., Azhar Chishti, M., Horne, P., Heslin, D., French, J., Mount, H. T. J., Nixon, R. A., Mercken, M., Bergeron., C., Fraser, P. E., St. Geoge-Hyslop, P., and Westaway, D. (2000) *Nature 408*, 979−982.
9. Kelly, J. W. (1998) *Curr. Opin. Struct. Biol. 8*, 101−106.
10. Jarrett, J. T., Berger, E. P., and Lansbury, P. T., Jr. (1993) *Biochemistry 32*, 4693−4697.
11. Jarrett, J. T., and Lansbury, P. T., Jr. (1993) *Cell 73*, 1055−1058.
12. Harper, J. D., and Lansbury, P. T., Jr. (1997) *Annu. Rev. Biochem. 66*, 385−407.
13. Naiki, H., and Nakakuki, K. (1996) *Lab. Invest. 74*, 374−383.
14. Lomakin, A., Chung, D. S., Benedek, G. B., Kirschner, D. A., and Teplow, D. B. (1996) *Proc. Natl. Acad. Sci. U.S.A. 93*, 1125−1129.
15. Esler, W. P., Stimson, E. R., Ghilardi, J. R., Vinters, H. V., Lee, J. P., Mantyh, P. W., and Maggio, J. E. (1996) *Biochemistry 35*, 749−757.
16. Eslar, W. P., Stimson, E. R., Ghilardi, J. R., Felix, A. M., Lu, Y. A., Vinters, H. V., Mantyh, P. W., and Maggio, J. E. (1997) *Nat. Biotechnol. 15*, 258−263.
17. Esler, W. P., Stimson, E. R., Jennings, J. M., Vinters, H. V., Ghilardi, J. R., Lee, J. P., Mantyh, P. W., and Maggio, J. E. (2000) *Biochemistry 39*, 6288−6295.
18. Myszka, D. G., Wood, S. J., and Biere, A. L. (1999) *Methods Enzymol. 309*, 386-402.
19. Myszka, D. G. (2000) *Methods Enzymol. 323*, 325−340.
20. Bradford, M. M. (1976) *Anal. Biochem. 72*, 248−254.
21. Stenberg, E., Persson, B., Roos, H., and Urbaniczky, C. (1991) *J. Colloid Interface Sci. 143*, 513−526.
22. Kusumoto, Y., Lomakin, A., Teplow, D. B., and Benedek, G. B., (1998) *Proc. Natl. Acad. Sci. U.S.A. 95*, 12277−12282.
23. Hardy, J., and Selkoe, D. J. (2002) *Science 297*, 353−356.
24. Kanai, M., Matsubara, E., Isoe, K., Urakami, K., Nakashima, K., Arai, H., Sasaki, H., Abe, K., Iwatsubo, T., Kosaka, T., Watanabe, M., Tomidokoro, Y., Shizuka, M., Mizushima, K., Nakamura, T., Igeta, Y., Ikeda, Y., Amari, M., Kawarabayashi, T., Ishiguro, K., Harigaya, Y., Wakabayashi, K., Okamoto, K., Hirai, S., and Shoji, M. (1998) *Ann. Neurol. 44*, 17−26.
25. Funato, H., Yoshimura, M., Kusui, K., Tamaoka, A., Ishikawa, K., Ohkoshi, N., Namekata, K., Okeda, R., and Ihara, Y. (1998) *Am. J. Pathol. 152*, 1633−1640.
26. Iwata, N., Tsubuki, S., Takaki, Y., Shirotani, K., Lu, B., Gerard, N. P., Gerard, C., Hama, E., Lee, H. J., and Saido, T. C. (2001) *Science 292*, 1550−1552.

BI020369W